SCIENTIFIC REPORTS

OPEN

SUBJECT AREAS:
CHEMICAL ENGINEERING
NANOPARTICLES
CHEMICAL BONDING
NANOPORES

Received
28 November 2012

Accepted
22 March 2013

Published
10 April 2013

Correspondence and requests for materials should be addressed to J.C.D.D.C. (j.dacosta@uq.edu.au)

# Reversible Redox Effect on Gas Permeation of Cobalt Doped Ethoxy Polysiloxane (ES40) Membranes

Christopher R. Miller, David K. Wang, Simon Smart & João C. Diniz da Costa

The University of Queensland, FIMLab – Films and Inorganic Membrane Laboratory, School of Chemical Engineering, Brisbane, QLD 4072, Australia.

**This work reports the remarkable effect of reversible gas molecular sieving for high temperature gas separation from cobalt doped ethoxy polysiloxane (CoES40) membranes. This effect stemmed from alternating the reducing and oxidising (redox) state of the cobalt particles embedded in the ES40 matrix. The reduced membranes gave the best $H_2$ permeances of $1 \times 10^{-6}$ mol $m^{-2}$ $s^{-1}$ $Pa^{-1}$ and $H_2/N_2$ permselectivities of 65. The reduction process tailored a molecular gap attributed to changes in the specific volume between the reduced cobalt ($Co(OH)_2$ and CoO) particles in the ES40 structure, thus allowing for the increased diffusion of gases. Upon re-oxidation, the tailored molecular gap became constricted as the particles reversed to $Co_3O_4$ resulting a lower gas diffusion, particularly for the larger gases ie. $CO_2$ and $N_2$. The ES40 matrix proved to be structurally rigid enough to withstand the reversible redox effect of cobalt particles across multiple cycles.**

The development of silica derived membranes has been specifically targeted to the tailoring of pore sizes to molecular sieving dimensions. A key feature of this development has been the employment of tetraethylorthosilicate (TEOS) as the silica precursor which gives immense flexibility in the sol-gel synthesis, and is one of the precursor compounds of the ethyl silicate family. For instance, the silica condensation reactions can be partially inhibited by low water to silica molar ratio, thus reducing the generation of siloxane bridges (Si-O-Si) in favor of silanols. As a result, molecular sieve silica structures are formed with pore sizes ~3Å[1], which are intrinsically related to the weakly branched fractal dimensions containing a high concentration of uncondensed silanol (Si-OH) species[2]. Subsequently, structural tailoring of silica membranes has been explored by the use of organic templates such as embedding and carbonizing ionic surfactants[3] in the silica matrix, or the development of hierarchical membranes using non-ionic surfactants[4,5]. An additional development led to the doping of metal oxides into silica films[6–8]. This has been of particular interest in the field of membranes to improve the chemical stability and long term operation in excess of 2000 hours[9].

By itself, pure microporous silica derived from TEOS has a trimodal pore distribution determined from positron annihilation spectroscopy PALS[10]. Hence, gas diffusion into amorphous silica membranes is generally controlled by a percolative porous pathway containing smaller pore diameters in the region of 3Å. In similar fashion, Uhlmann *et al.*[11] recently exposed cobalt oxide silica membranes to $H_2S$, and found no reaction between the sulphur-philic cobalt oxide and $H_2S$. Therefore, the pore sizes of amorphous silica around cobalt oxide particles are likewise around 3Å.

The use of silica precursors has not been exclusively limited to TEOS for the preparation of silica membranes. Other precursors used include methyltriethoxysilane[12,13], and octyl-, dodecyl- or octadecyltriethoxysilane[14]. These organic pendant groups covalently linked to the silica backbone are hydrophobic in nature which is believed to confer some structural stability to the silica matrix. Recently, hybrid silica derived from organic-inorganic groups such as hexaethoxy disiloxane[15], bis(triethoxysilyl)methane[16], bis(triethoxysilyl)ethane[17–19], and 1,1,3,3-tetraethoxy-1,3-dimethyl disiloxane[20] have also been used. The organic bridging groups that are linked between the silica atoms are commonly known as the organic spacers. By changing the silica precursor with a different spacer group, it was reported[17] that the network pore size can be tailored which has the ability to preferentially separate molecules based on their molecular size and affinity.

An alternative precursor of the ethyl silane family is the partially condensed TEOS, ethoxy polysiloxane $(Si(OC_2H_5)_2)_n$ or commonly known as ES40. This precursor is available commercially, which is industrially derived from TEOS using 40% of the theoretical water concentration, therefore it has 40% of silica by mass[21], or

60% of the alkoxide groups. Fig. S1 (supplementary information) shows the chemical structure of ES40 and TEOS for comparison. The potential advantage of using ES40 is closely related to the existing mixture of oligomers, thus avoiding pre-hydrolysis of TEOS in the preparation of silica membranes.

In this paper, we report the first use of silica precursor of ES40 for the synthesis of cobalt oxide microporous silica (CoES40) membrane. Of particular interest, it was remarkable to observe that the membranes exhibited the reversible gas permeation behaviour based on its thermal and redox properties. The cobalt silica xerogels were characterized using nitrogen gas adsorption, Fourier transform infra-red–attenuated total reflectance, micro-Raman and x-ray photoelectron spectroscopies. Finally, CoES40 sol-gel solution was used to prepare the top layer of asymmetric membrane on ceramic supports to demonstrate the thermal-chemical reversible effect of its molecular sieving performance for gas separation.

## Results

The spectroscopic investigations of the xerogel samples before and after reduction are shown in Fig. 1. Firstly, FTIR analysis of the CoES40 xerogels in Fig. 1a shows bands near 800, 1080 and 1200 $cm^{-1}$ assigned to siloxane bonds and at 950 $cm^{-1}$ to silanol bonds. Reduction of CoES40 xerogels confirmed the loss of the $Co_3O_4$ peak near 670 $cm^{-1}$ after hydrogen treatment, despite no peak relating to the intermediate species of cobalt oxides being observed. Also supported by Raman, spectra of the as prepared sample (Fig. 1b) verified the presence of $Co_3O_4$ from strong vibrations attributed to the $A_{1g}$, $E_g$ and $F_{2g}$ modes observed at 670, 471 and 181 $cm^{-1}$ with bands of lesser intensity at 605 and 512 $cm^{-1}$ for $F_{2g}$ modes[22]. Furthermore, the Raman spectrum of the hydrogen reduced CoES40 xerogel is dominated by an intense highly polarized band near 520 $cm^{-1}$. This band is attributed to the CoO ($A_g$) symmetric stretching mode of the $Co(OH)_2$ from the reduction of the $Co_3O_4$[22]. On a closer inspection of this band, there is a shoulder band near 460 $cm^{-1}$ which is assigned to a OCoO bending mode of the $Co(OH)_2$[22,23].

However, FTIR and Raman spectroscopy cannot pick up vibrations assigned to Co metal. Hence, XPS analysis was carried out to further provide evidence of the redox state of cobalt particles embedded into the ES40 matrix. In Fig. 1c, high-resolution Co 2p spectra of the cobalt species show $2p_{1/2}$ and $2p_{3/2}$ components due to spin-orbit splitting which qualitatively contains the same chemical information[24]. Therefore in this study, the higher intensity Co $2p_{3/2}$ component was curve-fitted, including the shake-up satellites of the $Co^{2+}$ ions. In the Co 2p spectrum of the as prepared CoES40 xerogel (Fig. 1c), $Co_3O_4$ species shows two main peaks at 779.5 and 781 eV which belong to Co(III) and Co(II) oxidation states respectively. In the higher binding energy (BE) region, the presence of the multiple electron excitation, commonly known as the shake-up satellites can be observed near 785 eV[25]. It is commonly used to distinguish the elemental compositions between Co(II) oxides and Co(III) oxides because the latter do not have the multiple electron excitations. When the $Co_3O_4$ species were reduced by hydrogen, the curve-fitting analysis in Fig. 1c shows only the Co(II) peak at 780.6 eV which indicates that all the cobalt (III) species in the xerogel were reduced to the Co(II) species. The position of this main peak attributing to the Co(II) of the $Co(OH)_2$ and CoO species is in good agreement with the XPS results reported by Yang *et al.*[22] and Biesinger *et al.*[26]. Additionally, the relative proportion of the shakeup satellites is also observed to increase dramatically after reduction which confirms the increase of the Co(II) species in the reduced xerogel. More importantly, the presence of the Co metal peak which typically occurs in the lower BE region at 778.1 eV[26] was not observed in the reduced xerogel.

The $N_2$ isotherm results of the CoES40 xerogels before and after hydrogen reduction are shown in Fig. S2 (supplementary information). The structure of both the xerogels is microporous as shown by the Type I isotherms with no hysteresis. However, as reflected by the decreased volume in the isotherm of the reduced xerogel, the reduction process lead to the loss in surface area and in total microporous volume ~50 $cm^2$ $g^{-1}$ and ~0.03 $cm^3$ $g^{-1}$ respectively. Essentially both reduced and oxidised samples demonstrated the formation of microstructures, a feature required for the preparation of silica membranes. Although the underlying physics and chemistry that govern silica polymeric growth and gelation are essentially the same for films as bulk gels, one must bear in mind that there are other factors that influence structural evolution in films[2,27]. For instance, the properties of a deposited thin film may be quite different from bulk gels due to non-equivalent gelation and drying conditions[28]. Nevertheless, there is a strong correlation between microporous bulk gel leading to the preparation of molecular sieving membranes, and the bulk gel results are generally considered qualitative[29].

The permeation results of single gases as a function of temperature for the CoES40 membranes are shown in Fig. 2. For the reduced membranes (Fig. 2a), the permeance for $H_2$ increased linearly with temperature reaching a maximum value of $1 \times 10^{-6}$ mol $m^{-2}$ $s^{-1}$ $Pa^{-1}$ at 450°C. The $H_2$ permeance shows a slight upturn at ~350°C, which is clearly evident for a greater upturn in $CO_2$ and $N_2$ permeance at the same temperature. The observed upturn in permeation is unusual for silica derived membranes having molecular sieve properties. In contrast, this trend does not repeat itself for the $CO_2$ and $N_2$ permeance for the oxidised membrane in Fig. 2b.

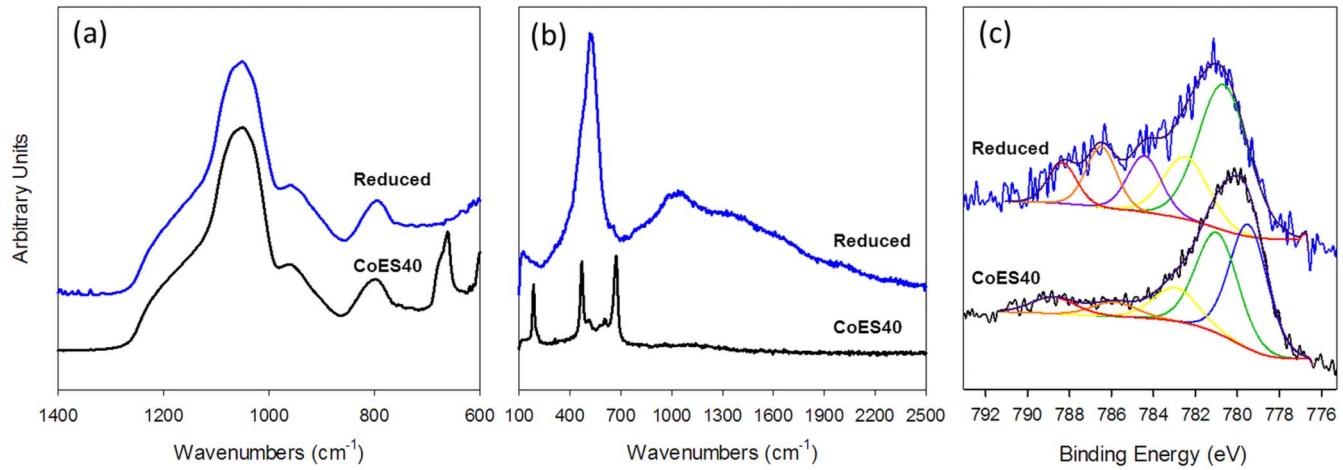


**Figure 1** | **(a) ATR-FTIR, (b) micro-Raman and (c) XPS spectra of the as prepared (black curve) and hydrogen reduced (blue curve) CoES40 xerogels.**

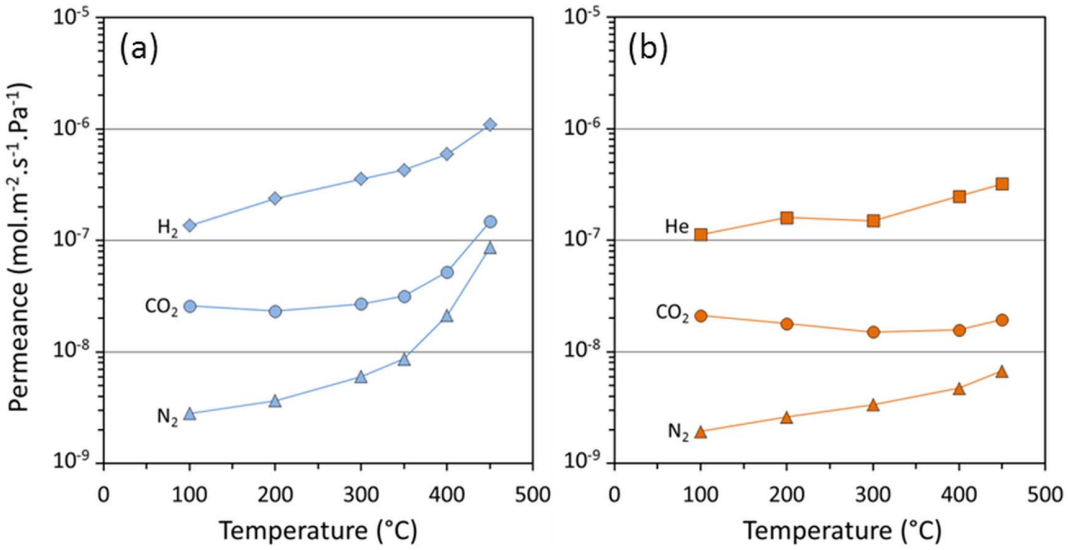


**Figure 2** | **Single gas permeances of the (a) reduced in blue data and (b) oxidised in orange data of the CoES40 membrane.**

Comparing both membranes, the reduced CoES40 membrane delivered higher $H_2$ permeance than the He permeance in the oxidised membrane, whilst the $CO_2$ and $N_2$ permeances were similar up to 300°C. As the molecular kinetic diameter of He ($d_k = 2.6$Å) is smaller than $H_2$ ($d_k = 2.89$Å), it would be expected that He permeance would be higher than that of $H_2$.

The permeation behavior of the CoES40 membranes is further highlighted by the gas permselectivities in Fig. 3. In the absence of reduction, the permselectivity of $He/N_2$ is found to be approximately 45 to 60 across all temperatures tested without any significant differences. However, by testing the reduced membrane, the permselectivity of $H_2/N_2$ decreased rapidly from 65 to 12 at 200 to 450°C, respectively. Interestingly, between 100 and 300°C the selectivity of $He/N_2$ of the oxidised membranes are observed to be lower and a crossover can be estimated in the temperature region near 350°C. Another important point is that both membranes delivered reasonable $CO_2/N_2$ permselectivities up to 11 in Fig. 3. These results are uncommon for silica derived membranes.

A key feature and remarkable finding of this work was the ability of the CoES40 membrane to consistently and reversibly switch its gas permeation from a reduced to an oxidizing state as clearly demonstrated in Fig. 4. In this particular experiment, the CoES40 membrane was pre-conditioned overnight at 450°C with the helium or hydrogen gases. The single gas permeances for the reduced membranes are in the region of $1.1 \times 10^{-6}$, $1.5 \times 10^{-7}$ and $8.6 \times 10^{-8}$ mol $m^{-2}$ $s^{-1}$ $Pa^{-1}$ for He, $CO_2$ and $N_2$, respectively. Likewise, their respective permeance values decrease to $\sim 7.3 \times 10^{-7}$, $4.4 \times 10^{-8}$ and $1.8 \times 10^{-8}$ mol $m^{-2}$ $s^{-1}$ $Pa^{-1}$ when the membranes were oxidised. This gas permeance evolution was highly reproducible and reversible over the six cycles using the same membrane under continuous permeation testing. These results have never been previously reported for amorphous silica membranes. The only published work to date demonstrating this switchable permeation performance is on crystalline ceramic membranes based on vanadium aluminium phosphates on alumina substrates[30]. The average selectivities of $He/N_2$ were 40 and 13 when switching from oxidised to reduced state, respectively. It was found that the long term conditioning in helium caused oxidation of the CoES40 matrix for temperatures above 350°C. In order to confirm this point, the reduced xerogel was pre-conditioned solely in helium gas, after which the sample

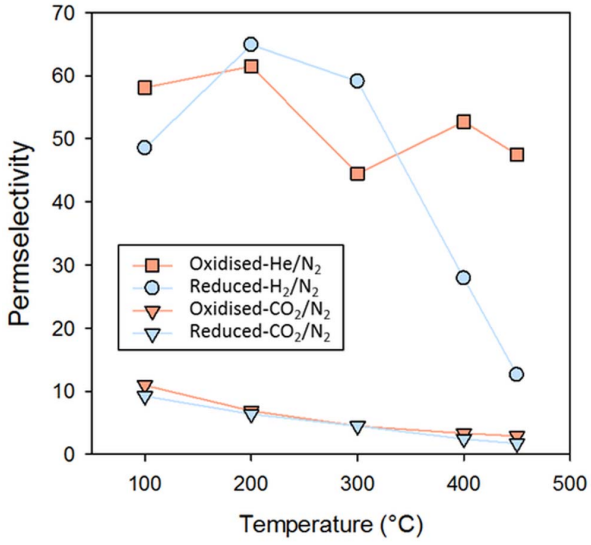


**Figure 3** | **Gas permselectivities as a function of temperature for the reduced (blue) and oxidised (orange) CoES40 membrane.**

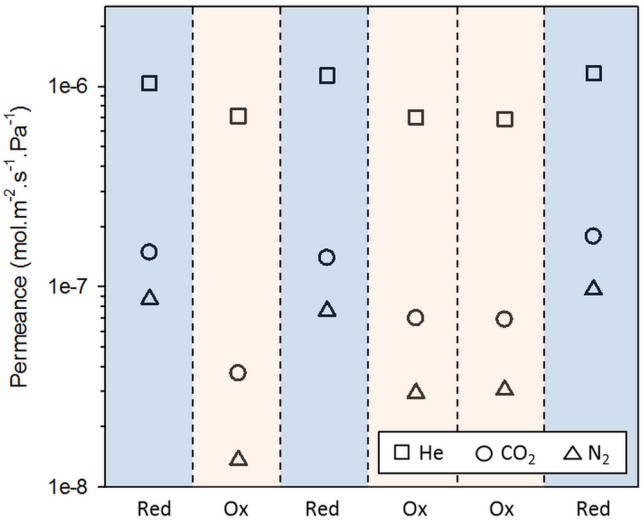


**Figure 4** | **Reversible redox cycling effect in single gas permeance at 450°C for the reduced and the oxidised state of the CoES40 membrane.**

was immediately analyzed spectroscopically to confirm the re-oxidation reaction. Figs. S3a, b and c (supplementary information) exhibiting the FTIR, Raman and XPS spectra clearly revealed the re-emergence of the $Co_3O_4$ species in the re-oxidised CoES40 xerogel, matching the results in Fig. 1. Hence, the reduced sample was fully re-oxidised under helium condition which corroborated with the reversible gas permeation results as demonstrated in Fig. 4.

## Discussion

The gas permeation behaviour of the CoES40 membranes is completely uncharacteristic of cobalt silica membranes in the literature which are typically prepared from TEOS as the precursor[6,9,31,32]. In these reports, the molecular sieve silica effect give temperature dependent transport through CoTEOS membranes such as the permeance of He and $H_2$ increases with temperature while $CO_2$ and $N_2$ permeance decreases. In the low temperature region up to 300°C, the CoES40 membranes follow this molecular sieve patterns for $H_2$, He and $CO_2$ transport, but not for $N_2$, irrespectively as to whether the membrane was oxidised or reduced. When the membrane was in reduced state for high temperatures in excess of 350°C (see Fig. 2a), there is a large increase in the permeance for $CO_2$ and $N_2$, whilst $H_2$ was moderate. These results are significant and thus suggest structural changes in the CoES40 matrix.

In molecular sieving, the structure of the membrane matrix and gas transport properties is intrinsically linked. In Fig. 2a, the $N_2$ permeance increased by one order of magnitude and $CO_2$ by three fold as the temperature raised from 350 to 450°C. This means that the incremental heat energy added to the membrane system allowed for a large and significant increase in the gas permeance. For this to happen, the average pore sizes, or pore constrictions in the CoES40 percolation pathways, have enlarged sufficiently to allow for a high permeation of the larger penetrant gases $CO_2$ ($d_k$ = 3.3 Å) and $N_2$ ($d_k$ = 3.64 Å). Hence, these results strongly indicate that the reduction of cobalt tetroxides to cobalt hydroxides and oxides embedded into the matrix of ES40 formed an extra molecular gap in the membrane matrix as schematically represented in Fig. 5. This representation is in principle counter-intuitive, as Fig. S2 (supplementary information) shows that the surface area and pore volume slightly decreased for the reduced sample. However, one must bear in mind that the $N_2$ sorption results are normalised per gram of sample. The density of

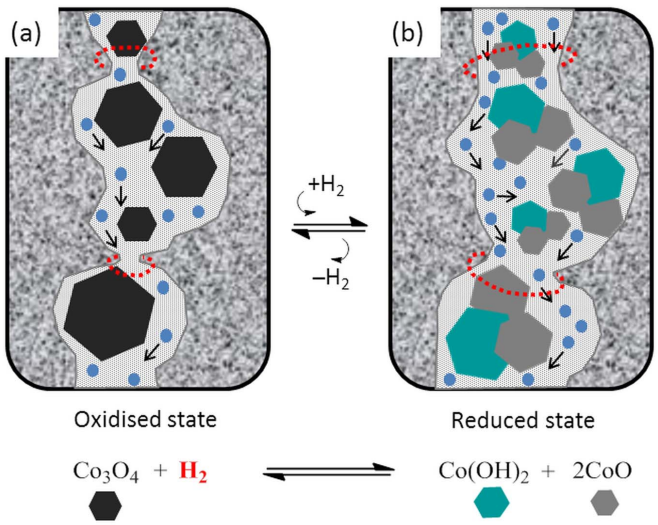


**Figure 5 | Schematic representation of the CoES40 matrices illustrating pore size and diffusion of single gas penetrants for (a) the oxidised and (b) the reduced membranes where each $Co_3O_4$ (black) is reduced to a $Co(OH)_2$ (green) and two CoO (grey) particles.** The red halos represent the location and the enlargement of the molecular gap.

$Co_3O_4$ is 6.1 g cm$^{-3}$ and of the reduced $Co(OH)_2$ and 2CoO is 16.4 g cm$^{-3}$ [33]. Based on the densities and the 25% molar ratio of cobalt in the xerogels, the reduced sample is 67% heavier than the oxidized sample. If the $N_2$ sorption was normalised by volume instead of weight, the reduced sample would therefore have a larger pore volume and surface area than the oxidised sample. The oxidised matrix in Fig. 5a shows smaller pore sizes and cobalt tetraoxide nanoparticles, which form smaller constrictions for gas diffusion. Upon reduction, Fig. 5b depicts the enlargement of the pore sizes attributed to the phase change of the cobalt tetraoxide particles as described by equation 1 and confirmed by the spectroscopic results in Fig. 1. The tailored molecular gap causes the widening of the pore sizes (see red halos in Fig. 5b) which correlates well with the increase in permeation for the large kinetic diameter gases ($N_2$ and $CO_2$) in Fig. 2a, and the lowering of $H_2/N_2$ permselectivity in Fig. 3, particularly at high temperatures.

Another interesting aspect of the CoES40 membranes is their ability to separate $CO_2$ from $N_2$. In Figs. 3, it is observed that the $CO_2/N_2$ permselectivity increases from 2 to 11, as the temperature reduces from 350 to 100°C, respectively. Again this performance behavior is uncharacteristic of CoTEOS and other types of silica membranes as $CO_2/N_2$ permselectivity is generally below 2[6,9,31,32]. Higher values (>25) have been reported for CVD (Chemical Vapour Deposition) prepared membranes only[34]. These results strongly suggest that the CoES40 formed a trimodal pore size distribution where there are percolation pathways (i) with pore sizes around 3 Å which separate He or $H_2$ from larger gas molecules, (ii) pore sizes between 3.3 and 3.64 Å which allows for diffusion of $CO_2$, but hindering the passage of $N_2$, and (iii) a small proportion of pore sizes slightly larger than 3.64 Å reflected by the low $N_2$ permeance.

Therefore, both of the cobalt oxides and the ES40 precursor played an important role in the reversible molecular sieving effect for gas permeation and separation. Firstly examining the role of cobalt oxides, the reduction process resulted in the formation of Co(II) as evidenced by the XPS analysis, which also corroborate with the Raman analysis. To be more specific, the reduction of cobalt oxide in the form of $Co_3O_4$ at high temperatures (>350°C) produces thermodynamically-unstable intermediates in the form of $Co(OH)_2$ and CoO (equation 1)[35,36]. This pathway was clearly evidenced by the presence of the $Co(OH)_2$ species in the infrared and the Raman spectra (Fig. 1a and b), in addition to $Co(OH)_2$ and CoO in the XPS spectrum (Fig. 1c) of the reduced CoES40 xerogel.

$$Co_3O_4 + H_2 \rightleftarrows Co(OH)_2 + 2CoO \qquad (1)$$

Indeed, hydrogen reduction of the $Co_3O_4$ resulted in a complete change in the composition of the silica matrix which can be related to its physical properties, as also evidenced by the surface area and pore volume in Fig. S2 (supplementary information). From the respective densities of the $Co(OH)_2$, CoO, and $Co_3O_4$ is 3.6, 6.4 and 6.1 g cm$^{-3}$ [33], the specific molar volume of the reduced species as per equation 1, is thus calculated to be 0.05 cm$^3$ mmol$^{-1}$ which is 1.2 times greater than that of $Co_3O_4$ at 0.04 cm$^3$ mmol$^{-1}$. As a consequence, the occupied volume of the cobalt compounds in the silica matrix increases when the membrane was exposed to hydrogen, thus causes the molecular gap nearby the reduced cobalt compounds to enlarge as schematically shown in Fig. 5.

By the same token, the re-oxidation of the $Co(OH)_2$ and CoO to $Co_3O_4$ has the opposite effect in terms of specific volume. This directly leads to diminishing the tailored molecular gap between the cobalt oxide particles and the ES40 structure. The re-oxidation process was attributed to the removal of $H_2$ gas from the reduced cobalt species as seen in equation 1. In the absence of $H_2$, the equilibrium is shifted in favour of the more thermodynamically-stable oxidised $Co_3O_4$ particles from the metastable reduced cobalt species. Hence, when the membrane was pre-conditioned in He gas at 450°C for an

extend period of time, the re-oxidation of the cobalt compounds occur as confirmed by the results the spectroscopic analyses using FTIR, Raman and XPS (Fig. S3). These results strongly indicate that the cobalt species present inside the silica matrix are readily undergoing redox reactions in the presence or absence of $H_2$. Hence, the redox reactions delivered a reversible molecular gap tailoring where the permeance of gases can increase or decrease according to the oxidation state of the cobalt oxide particles as evidenced by Fig. 4.

This reversible effect has never been reported for pure silica or cobalt TEOS membranes. Such results suggest that TEOS derived matrices may encase the cobalt oxide particles in a non-rigid fashion, mainly because these membranes contain a large amount of silanol groups which tend to be collapsible, weakly branched structures. Hence, any redox variation in TEOS derived membranes does not deliver the reversible gas behaviour as observed for the membranes prepared with ES40 precursors. In addition, the ES40 membrane in this work was prepared using a different sol-gel synthesis than those membranes derived from TEOS. As ES40 is a partially condensed silica precursor, the CoES40 xerogel was synthesized without given any extended hydrolysis time which typically involves 3 hours of reaction time during the sol-gel preparation. In addition, no oxidant or acid reagent such as hydrogen peroxide or nitric acid was added into the sol mixture as they are common reagents required for catalyzing the hydrolysis step. This is a major difference between using ES40 and TEOS in the preparation of silica films. Hence, ES40 amorphous structure is distinct from the conventional synthesized silica membranes.

This can be rationalized by the different growth mechanism of the silica during the sol-gel processes of ES40 and TEOS on the basis of the polymer growth in silicate systems as described by Martin[37] and Schaefer[38]. The fact that the ES40 precursor as silicate oligomers are predominately $Q^1$ and $Q^2$ species, which are more acidic than $Q^0$ species in the TEOS precursor, the evolving structures of the silicate are expected to be vastly different between ES40 and TEOS precursors. In the absence of the $Q^0$ monomers, condensation occurs preferentially between the $Q^1$ species and the more acidic $Q^2$ species where the chain terminals react with chain pendants, respectively[2]. As a consequence, the tendency for the structures to undergo cluster-cluster growth to form very open fractal structures due to a higher degree of condensation is greater in the ES40 sol-gel process. In the $^{29}$Si magic-angle spinning NMR study of the silica xerogels, Mrowiec-Bialoń *et al.*[21] presented that the population of $Q^3$ and $Q^4$ sites predominated the silica structure in the xerogels prepared by ES40 than that of the TEOS which can only be explained by a greater silanol condensation. They further made postulations from the SAXS results that ES40 xerogels appear to have a higher microstructural homogeneity indicating a thicker and stronger polymeric network which consisted of a highly condensed silica wall on one side with a thick polymeric chain barrier on the other, whereas the TEOS xerogels resulted in a lower homogeneity suggestive of a thinner polymeric chain wall. Further, ES40 xerogels exhibit larger pore size and micropore volume but lower surface area of silica xerogels than those observed in the corresponding TEOS sol-gel formulation[21,39].

These examinations match very closely with the permeation results in this work. For instance the oxidised CoES40 membrane its $H_2$ permeance was up to 5 times higher than that of a similar CoTEOS membrane[9], though the $He/N_2$ permselectivities was reduced by 20 fold. These results correlate well with the pore size and pore volume increase, though the ES40 sol-gel process still tailored molecular sieving structures based on permselectivities of up to 69. In addition, the reversible redox effect can occur only in the case of the silica backbone structure that is rigid enough to oppose collapse upon changes in the redox state of the cobalt particles. The ES40 structure has proven that this is the case, mainly attributed to a stronger fractal branched system derived from an initial partially condensed silica precursor.

## Methods

**Sol-gel preparation and characterization.** CoES40 xerogel samples were prepared using a simplified sol-gel method. Cobalt nitrate hexahydrate ($Co(NO_3)_2.6H_2O$; 98%, Alfa Aesar) was dissolved in double distilled water, diluted with ethanol (EtOH; AR grade), and ES40 (ES40; Colcoat Co., Japan) was slowly added under stirring to achieve a final molar ratio of 255 : 4 : 1 : 40 for the EtOH : ES40 : $Co(NO_3)_2.6H_2O$ : $H_2O$ sol. After 10 mins of mixing at room temperature, the sol was dried in an oven at 60°C for 96 hours. Dried samples were ground to a fine powder and calcined in an air atmosphere in a temperature-controlled furnace at 630°C, with a hold time of 2.5 hours and a heating/cooling rate of 1°C $min^{-1}$.

For hydrogen reduction, the xerogel samples were treated at 550°C for 10 hours at a heating/cooling rate of 5°C $min^{-1}$ in hydrogen flow (40 mL $min^{-1}$). After the xerogels were reduced, the pre-conditioning experiment was carried out at 450°C for 10 hours at a heating/cooling rate of 5°C $min^{-1}$ in helium flow (40 mL $min^{-1}$) for the re-oxidation reaction to take place.

Fourier transform infra-red – attenuated total reflectance (FTIR-ATR) characterization was performed on a Shimadzu IRAffinity-1 with a PIKE MIRacle single-bounce diamond crystal plate accessory. FTIR spectra were recorded over a wavelength range of 1400–600 $cm^{-1}$. X-ray photoelectron spectrometry (XPS) was carried out using a Kratos Axis ULTRA XPS incorporating a 165 mm hemispherical electron energy analyzer. The incident radiation was monochromatic Al Kα X-rays (1486.6 eV) at 225 W (15 kV, 15 mA) and at 45° to the sample surface. The data was collected at take-off angle of $\theta = 90°$. Survey scans over 1200–0 eV binding energy range with 1.0 eV steps and a dwell time of 100 ms were taken at an analyzer pass energy of 160 eV. The high resolution scans of Co 2p, O 1s, and Si 2p were taken with 0.05 eV steps and 250 ms dwell time at pass energy of 20 eV. Nitrogen gas adsorption measurements were carried out in triplicate samples degassed for a minimum of 6 h to a pressure of 2 Pa at 200°C in a Micromiretics VacPrep061 prior to analysis by a Micromeritics Tristar 3000 analyzer. Specific surface area and micropore volume measurements were determined by the Brunner-Emmett-Teller (BET). Raman spectra were acquired with a Nicolet Almega XR dispersive Raman spectrometer coupled to an Olympus microscope using a He : Ne laser (633 nm) over 3900–70 $cm^{-1}$.

**Membrane preparation and testing.** Thin CoES40 films were coated on tubular alumina supports (10 mm i.d., 14 mm o.d., 100 mm length) consisting of α–alumina substrate and γ–alumina interlayer were obtained from the Energy Research Centre of the Netherlands (ECN). ECN tubular alumina supports were first rinsed with ethanol and dried in an air-oven at 60°C before dip-coating with the CoES40 sol. Each layer was deposited onto the supports using a dip-coater with a dwell time of 1 min and a withdrawal rate of 10 cm $min^{-1}$. After the deposition of each layer, the membranes were dried at 60°C for 1 hour in an oven and were calcined in an air atmosphere in a temperature controlled oven at 630°C, with a hold time of 2.5 h and a heating/cooling rate of 1°C $min^{-1}$. The cycle of dip-coating and calcinations was repeated three times to achieve a total of three top layers. After calcination, the outer surface of the membranes had a distinctive dark olive green color.

The performance of each membrane was assessed by single gas permeance using a custom made rig described elsewhere[8]. The permeation tests were carried out using high purity gases He (99.996%), $H_2$ (99.999%), $CO_2$ (99.5%) and $N_2$ (99.99%). The permeation protocol was performed in the order for $H_2$, $N_2$, $CO_2$ gases for the reduced membranes, and He, $N_2$ and $CO_2$ for the oxidised membranes. The gas permeance (mol $m^{-2}s^{-1}Pa^{-1}$) was determined from a transient dead-end mode, based on the measurement of pressure (MKS pressure transducer) change in a known fixed volume linked to the membrane permeate stream.


1. Diniz da Costa, J. C., Lu, G. Q., Rudolph, V. & Lin, Y. S. Novel molecular sieve silica (MSS) membranes: characterisation and permeation of single-step and two-step sol–gel membranes. *J. Membr. Sci.* **198**, 9–21 (2002).
2. Brinker, C. J. & Scherer, G. W. *Sol-Gel Science : The Physics and Chemistry of Sol-Gel Processing.* (Academic Press, 1990).
3. Duke, M. C., Diniz Da Costa, J. C., Lu, G. Q., Petch, M. & Gray, P. Carbonised template molecular sieve silica membranes in fuel processing systems: Permeation, hydrostability and regeneration. *J. Membr. Sci.* **241**, 325–333 (2004).
4. Bosc, F., Ayral, A., Albouy, P. A., Datas, L. & Guizard, C. Mesostructure of anatase thin films prepared by mesophase templating. *Chem. Mater.* **16**, 2208–2214 (2004).
5. Yacou, C. *et al.* One pot synthesis of hierarchical porous silica membrane material with dispersed Pt nanoparticles using a microwave-assisted sol-gel route. *J. Mater. Chem.* **18**, 4274–4279 (2008).
6. Igi, R., Yoshioka, T., Ikuhara, Y. H., Iwamoto, Y. & Tsuru, T. Characterization of Co-doped silica for improved hydrothermal stability and application to hydrogen separation membranes at high temperatures. *J. Am. Ceram. Soc.* **91**, 2975–2981 (2008).
7. Kanezashi, M. & Asaeda, M. Hydrogen permeation characteristics and stability of Ni-doped silica membranes in steam at high temperature. *J. Membr. Sci.* **271**, 86–93 (2006).
8. Uhlmann, D., Liu, S. M., Ladewig, B. P. & da Costa, J. C. D. Cobalt-doped silica membranes for gas separation. *J. Membr. Sci.* **326**, 316–321 (2009).

9. Yacou, C., Smart, S. & Diniz da Costa, J. C. Long term performance cobalt oxide silica membrane module for high temperature H-2 separation. *Energ. Environ. Sci.* **5**, 5820–5832 (2012).
10. Duke, M. C., Pas, S. J., Hill, A. J., Lin, Y. S. & Diniz Da Costa, J. C. Exposing the molecular sieving architecture of amorphous silica using positron annihilation spectroscopy. *Adv. Funct. Mater.* **18**, 3818–3826 (2008).
11. Uhlmann, D., Smart, S. & da Costa, J. C. D. H(2)S stability and separation performance of cobalt oxide silica membranes. *J. Membr. Sci.* **380**, 48–54 (2011).
12. Raman, N. K. & Brinker, C. J. Organic 'template' approach to molecular sieving silica membranes. *J. Membr. Sci.* **105**, 273–279 (1995).
13. De Vos, R. M., Maier, W. F. & Verweij, H. Hydrophobic silica membranes for gas separation. *J. Membr. Sci.* **158**, 277–288 (1999).
14. Kusakabe, K., Sakamoto, S., Saie, T. & Morooka, S. Pore structure of silica membranes formed by a sol-gel technique using tetraethoxysilane and alkyltriethoxysilanes. *Sep. Purif. Technol.* **16**, 139–146 (1999).
15. Lee, H. R. *et al.* Pore-size-controlled silica membranes with disiloxane alkoxides for gas separation. *J. Membr. Sci.* **383**, 152–158 (2011).
16. Kanezashi, M., Kawano, M., Yoshioka, T. & Tsuru, T. Organic-inorganic hybrid silica membranes with controlled silica network size for propylene/propane separation. *Ind. Engineer. Chem. Res.* **51**, 944–953 (2012).
17. Kanezashi, M., Yada, K., Yoshioka, T. & Tsuru, T. Design of silica networks for development of highly permeable hydrogen separation membranes with hydrothermal stability. *J. Am. Chem. Soc.* **131**, 414–415 (2009).
18. Kanezashi, M., Yada, K., Yoshioka, T. & Tsuru, T. Organic-inorganic hybrid silica membranes with controlled silica network size: Preparation and gas permeation characteristics. *J. Membr. Sci.* **348**, 310–318 (2010).
19. Castricum, H. L. *et al.* Tailoring the separation behavior of hybrid organosilica membranes by adjusting the structure of the organic bridging group. *Adv. Funct. Mater.* **21**, 2319–2329 (2011).
20. Lee, H. R., Kanezashi, M., Shimomura, Y., Yoshioka, T. & Tsuru, T. Evaluation and fabrication of pore-size-tuned silica membranes with tetraethoxydimethyl disiloxane for gas separation. *Aiche Journal* **57**, 2755–2765 (2011).
21. Mrowiec-Białoń, J., Jarzębski, A. B., Pajak, L., Olejniczak, Z. & Gibas, M. Preparation and surface properties of low-density gels synthesized using prepolymerized silica precursors. *Langmuir* **20**, 10389–10393 (2004).
22. Yang, J., Liu, H., Martens, W. N. & Frost, R. L. Synthesis and characterization of Cobalt hydroxide, cobalt oxyhydroxide, and cobalt oxide nanodiscs. *J. Phys. Chem. C* **114**, 111–119 (2010).
23. Bøckman, O., Østvold, T., Voyiatzis, G. A. & Papatheodorou, G. N. Raman spectroscopy of cemented cobalt on zinc substrates. *Hydrometallurgy* **55**, 93–105 (2000).
24. Artyushkova, K., Levendosky, S., Atanassov, P. & Fulghum, J. XPS Structural studies of nano-composite non-platinum electrocatalysts for polymer electrolyte fuel cells. *Top. Catal.* **46**, 263–275 (2007).
25. McIntyre, N. S. & Cook, M. G. X-Ray photoelectron studies on some oxides and hydroxides of cobalt, nickel, and copper. *Anal. Chem.* **47**, 2208–2213 (1975).
26. Biesinger, M. C. *et al.* Resolving surface chemical states in XPS analysis of first row transition metals, oxides and hydroxides: Cr, Mn, Fe, Co and Ni. *Appl. Surf. Sci.* **257**, 2717–2730 (2011).
27. Brinker, C. J., Frye, G. C., Hurd, A. J. & Ashley, C. S. Fundamentals of sol-gel dip coating. *Thin Solid Films* **201**, 97–108 (1991).
28. Brinker, C. J., Hurd, A. J. & Ward, K. J. In *Ultrastructure Processing of Advanced Ceramics* (eds J. D. Mackenzie & D. R. Ulrich) 223–253 (Wiley, 1988).
29. Brinker, C. J. & Mukherjee, S. P. Comparisons of sol-gel-derived thin films with monoliths in a multicomponent silicate glass system. *Thin Solid Films* **77**, 141–148 (1981).
30. Farrusseng, D., Julbe, A. & Guizard, C. The first redox switchable ceramic membrane. *J. Am. Chem. Soc.* **122**, 12592–12593 (2000).
31. Battersby, S. *et al.* Performance of cobalt silica membranes in gas mixture separation. *J. Membr. Sci.* **329**, 91–98 (2009).
32. De Vos, R. M. & Verweij, H. Improved performance of silica membranes for gas separation. *J. Membr. Sci.* **143**, 37–51 (1998).
33. Patnaik, P. *Handbook of Inorganic Chemicals.* (McGraw-Hill, 2003).
34. Nakao, S. I., Suzuki, T., Sugawara, T., Tsuru, T. & Kimura, S. Preparation of microporous membranes by TEOS/O3 CVD in the opposing reactants geometry. *Microporous Mesoporous Mater.* **37**, 145–152, doi:10.1016/s1387-1811(99)00261-9 (2000).
35. Kababji, A. H., Joseph, B. & Wolan, J. T. Silica-supported cobalt catalysts for fischer-tropsch synthesis: Effects of calcination temperature and support surface area on cobalt silicate formation. *Catal. Lett.* **130**, 72–78 (2009).
36. Puskas, I. *et al.* Novel aspects of the physical chemistry of Co/SiO2 Fischer-Tropsch catalyst preparations. The chemistry of cobalt silicate formation during catalyst preparation or hydrogenation. *Appl. Catal., A* **311**, 146–154 (2006).
37. Martin, J. E. *Atomic & molecular processing of electronic and ceramic materials : preparation, characterization & properties : proceedings of the conference held August 30-September 2, 1987, University of Washington, Seattle, Washington, U.S.A.* 79–89 (Materials Research Society, 1987).
38. Schaefer, D. W. Fractal Models and the Structure of Materials. *MRS Bull.* **13**, 22–27 (1988).
39. Korach, Ł., Czaja, K., Mrowiec-Białoń, J. & Jarzebski, A. Effect of silica-type sol-gel carrier's structure and morphology on a supported Ziegler-Natta catalyst for ethylene polymerization. *Eur. Polym. J.* **42**, 3085–3092 (2006).


## Acknowledgements

The authors would like to acknowledge financial support provided by the Australian Research Council through Discovery Project Grant DP110101185. The Authors would like to thank the facilities and the scientific and technical assistance of Dr Barry Wood of the Australian Microscopy & Microanalysis Research Facility at the Centre for Microscopy and Microanalysis at The University of Queensland, and Dr Dana Martens for the Raman spectroscopy conducted at the Bio-Nano Development Facility in the Australian Institute for Bioengineering and Nanotechnology, which was funded by the Queensland State Government Smart State Innovation Building Fund.

## Author contributions

C.R.M. executed membrane preparation and testing. D.K.W. executed sol gel preparation and characterization, and performed results and analysis. D.K.W., S.S. and J.C.D.d.C. prepared and reviewed the manuscript.

## Additional information

**Supplementary information** accompanies this paper at http://www.nature.com/scientificreports

**Competing financial interests:** The authors declare no competing financial interests.



**How to cite this article:** Miller, C.R., Wang, D.K., Smart, S. & Diniz da Costa, J.C. Reversible Redox Effect on Gas Permeation of Cobalt Doped Ethoxy Polysiloxane (ES40) Membranes. *Sci. Rep.* **3**, 1648; DOI:10.1038/srep01648 (2013).